*Bulgarian Chemical Communications, Volume 47, Special Issue B (pp. 232–238) 2015*

# Hypernuclei reconstruction at NICA/MPD: a feasibility study

M. Ilieva*, V. Kolesnikov, D. Suvarieva, V. Vasendina, A. Zinchenko

*Veksler and Baldin Laboratory of High Energy Physics, Joint Institute for Nuclear Research, 141980 Dubna, Moscow region, Russia*

The study of production of light hypernuclei is essential for understanding the production mechanism of exotic objects such as multi-hypernuclei and can help us to understand strangeness degrees of freedom in hadronic system. This study shows the ability of the NICA/MPD complex to measure the lightest hypernucleus ${}^{3}_{\Lambda}$H.

**Key words:** hypernucleus, reconstruction, Monte Carlo, production, heavy-ion collisions, NICA/MPD

## INTRODUCTION

NICA (Nuclotron-based Ion Collider fAcility) is a new facility at the Join Institute for Nuclear Research [1]. The global goat of NICA is to study the behavior of nuclear matter under extreme conditions. A transition is expected of hot and dense baryon matter into a state of deconfined quarks and gluons - so called quark gluon plasma (QGP). In such matter phase transition might be accompanied by a restoration of chiral symmetry due to melting of the quark condensate [2–4]. Recent results on hadron-production from the CERN SPS [5] and RHIC [6] indicate that the onset of the deconfinement is likely to be observed in central A+A collisions at energies $\sqrt{s} = 4$ GeV. Moreover, the analysis of the thermodynamic freeze-out parameters extracted from the data over a wide energy range performed in [7] reveals that the net-baryon density in central collisions of heavy ions has a maximum in the energy range from $\sqrt{s} =$ 5A to 9A GeV. So, the energy range of the NICA collider ($4 < \sqrt{s} < 11$A GeV) is ideal for an experimental exploration of fundamental QCD properties that are sensitive to the both phenomena: chiral symmetry and confinement [8]. Our experimental research plan is to perform a detailed energy scan with ion beams from protons to gold nuclei addressing the following objectives: (1) strangeness production, (2) in-medium properties of vector mesons, (3) event-by-event fluctuations, and (4) correlations. The measurements will be performed with the MultiPurpose Detector (MPD) [9, 10] capable of detecting both the hadronic ($\pi$, $K$, $p$, $\Lambda$, $\Xi$, $\Omega$) and non-hadronic ($e$, $\gamma$) probes.

* To whom all correspondence should be sent:
maiailieva@mail.bg

Relativistic heavy-ion collisions where lots of strange particles (kaons and hyperons) are produced, offer a unique possibility to create exotic nuclear objects with strangeness - hypernuclei [11]. Recently, the first results on the production of (anti)hypertritium in relativistic Au+Au collisions at the RHIC and LHC were reported by the STAR and ALICE experiments [12, 13]. The mechanism and dynamics of hypernuclei formation is not well understood - several approaches are suggested to explain their production rates: coalescence of lambdas with nucleons at midrapidity [14], thermal models [15], or absorption of some of the produced hyperons by the residual spectator nuclei [16]. To distinguish between different models new experimental data on hyper-nuclei production taken in different initial conditions (i.e. collision energy and impact parameter) over large phase-space are needed.

The energy range of the NICA research program covers the region of the maximal baryon density where the production rates of nuclear clusters with strangeness are predicted to be enhanced considerably: as many as $3 \cdot 10^2$ of ${}^{3}_{\Lambda}$H and $10^{-5}$ of ${}^{5}_{\Lambda\Lambda}$He per unit of rapidity are expected in a central Au+Au collision at $\sqrt{s} = 5$A GeV [15]. With a typical event rate of 6 kHz for the design NICA luminosity of $10^{27}$ cm$^{-2}$c$^{-1}$ a detailed study of the production mechanism of single hypernuclei as well as an observation of double hypernuclei at NICA look feasible.

## DETECTOR GEOMETRY

The present analysis is based on the so-called start version of MPD, which includes the main tracker Time Projection Chamber (TPC) and barrel Time-Of-Flight system (TOF). The detectors cover the mid-rapidity region $|\eta| < 1.3$. The detailed description of the MPD geometry can be found in Refs. [9, 10].

## EVENT GENERATOR AND DATA SET

The event sample for the present study has ben produced with the DCM-QGSM (Dubna Cascade Model - Quark-Gluon String Model) generator [17–19]. The choice of this event generator was motivated by the fact that it can produce nuclear clusters via the coalescence mechanism and describe hypernuclei yield in NICA energy region. The DCM-QGSM generator is based on the Monte Carlo solution of a set of the Boltzmann- Uehling-Uhlenbeck relativistic kinetic equations with the collision terms, including cascade- cascade interactions. For particle energies below 1 GeV it considers only nucleons, pions and deltas. The model includes a proper description of pion and baryon dynamics for particle production and absorption processes. At energies higher than about 5 GeV, the Quark-Gluon String Model is used to describe elementary hadron collisions.

DCM-QGSM model predictions for cluster formation have been compared with experimental data [20, 21]. The model was used to predict cluster production over a wide range of beam energies [16].

For this study, the generator was used to produce a sample of central Au-Au collisions (0-3.8 fm) at $\sqrt{s}$ = 5A GeV. The number of events was $5{\cdot}10^5$ corresponding to about 30 minutes of NICA running time.

Particles produced by the event generators were transported through the detector using the GEANT3 transport package. The decay properties of hypernuclei (modes and branching ratios) have been introduced into GEANT from Ref. [22] (Tab. 1) and the lifetime has been taken to be the same as of Λ-hyperon.

Table 1. ${}^{3}_{\Lambda}$H decay modes and branching ratios. The studied ones are marked in bold

| Decay channel | Branching ratio,% |
|---|---|
| **$\pi^-$ + $^3$He** | **24.7** |
| $\pi^0$ + $^3$H | 12.4 |
| **$\pi^-$ + p + d** | **36.7** |
| $\pi^0$ + n + d | 18.4 |
| $\pi^-$ + p + p + n | 1.5 |
| $\pi^0$ + n + n + p | 0.8 |
| d + n | 0.2 |
| p + n + n | 1.5 |

## TRACK RECONSTRUCTION

The track reconstruction method is based on the Kalman filtering technique (see, e.g. [23]) and the number of TPC points per track was required to be greater than 10 to ensure a good precision of momentum and $dE/dx$ measurements. The track finding efficiency in TPC for primary and secondary tracks is shown in Fig. 1 (a) as a function of the track transverse momentum. The secondary track sample there included particles produced within 50 cm of the primary vertex both in transverse and longitudinal directions and did not include electrons and positrons from the photon conversion. The transverse momentum resolution as a function of $p_T$ can be seen in Fig. 1 (b). The result was obtained with the assumption on the TPC coordinate resolution of 0.5 and 1.0 mm in transverse and longitudinal directions, respectively.

Figure 2 (a) shows the transverse and longitudinal position uncertainties of primary tracks at their point of the closest approach to the interaction point versus track momentum. These detector characteris-

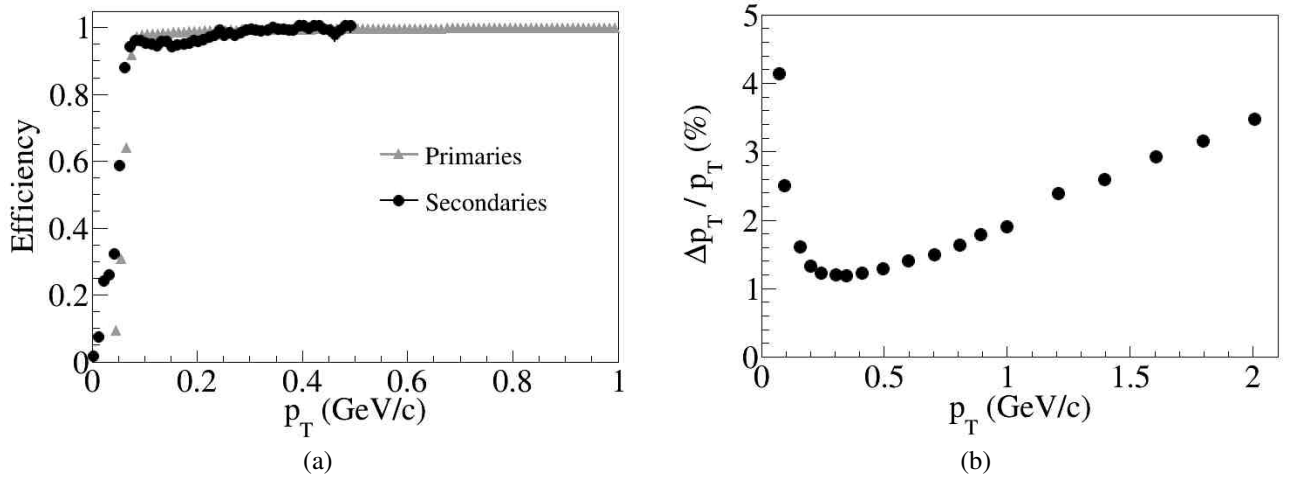


Fig. 1. (a) Track reconstruction efficiency as a function of track $p_T$ for primary and secondary particles. (b) Relative transverse momentum resolution for primary tracks with $|\eta| < 1.3$ reconstructed in TPC.

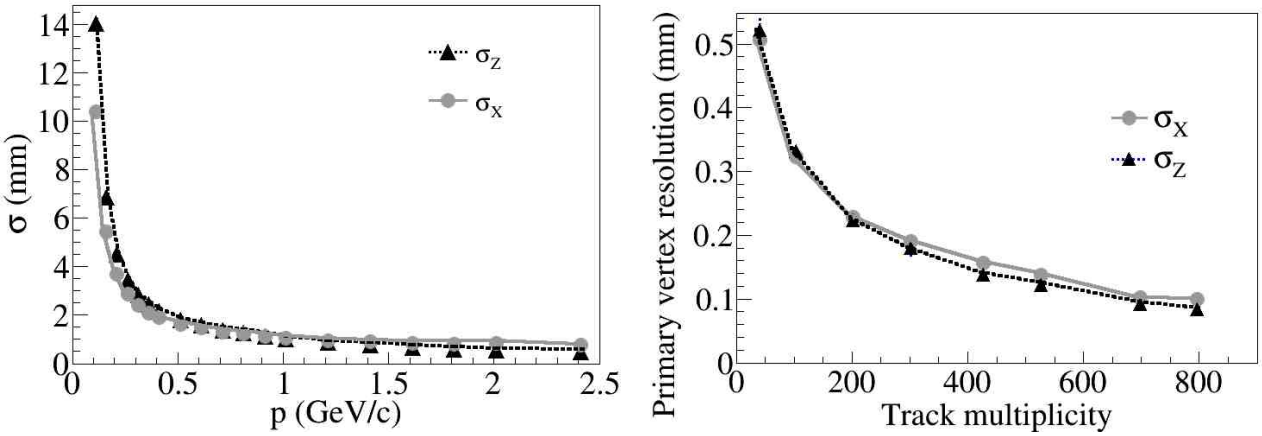


(a) (b)

Fig. 2. (a) Transverse and longitudinal position errors in the point of the closest approach (PCA) to the interaction point for TPC reconstructed primary tracks with $|\eta|$ <1.3 versus particle momentum; (b) Transverse and longitudinal position errors of the reconstructed primary vertex as functions of the track multiplicity.

tics are important for secondary vertex reconstruction. Both the primary and secondary vertex reconstruction methods utilized make use of the similar approach based on the Kalman filtering formalism [24]. The primary vertex reconstruction errors as functions of the track multiplicity in the event are shown in Fig. 2 (b).

For all the reconstructed in the TPC tracks the specific energy loss $dE/dx$ is calculated as a truncated mean of the charges of TPC hits assigned to the tracks. The truncation level of 70% was chosen, i.e. 30% of hits with the highest charges were excluded from the mean value. Next, the TPC reconstructed tracks are extrapolated to the TOF detector and matched to the TOF hits. For the matched candidates the mass square ($M^2$) is derived through the relation:

$$M^2 = (p/q)^2 \left( \frac{c^2 t^2}{l^2} - 1 \right)$$

where $p$ is the track momentum, $q$ is its charge, $t$ is the time-of-flight from TOF, $l$ is the path length from the collision vertex to the TOF hit, and $c$ is the speed of light. $p/q$, so-called magnetic rigidity, is the value directly returned by the track reconstruction algorithm. For particles with the unit charge it is equal to the momentum and $M^2$ corresponds to the particle mass.For multiple-charged particles the obtained value $M^2$ is scaled by the factor of $1/q^2$ with respect to the true mass s can be seen, e.g., in Fig. 1 for ${}^{3}_{\Lambda}$He (factor of $1/4$ with respect to the expected squared mass of 9).

## PARTICLE IDENTIFICATION

Particle identification (PID) in the MPD experiment will be achieved by energy loss ($dE/dx$) information from the TPC. As shown in Fig. 3 can discriminate kaons from pions up to momenta of 0.7 GeV/c and protons can be distinguished from $\pi$, $K$-mesons up to $p \approx 1.3$ GeV/c. Charged particles are selected if their $dE/dx$ measurement lies within a $3\sigma$ interval around the predicted value which is taken from the Bethe-Bloch parameterization for the mean energy loss [25].

Particles within the pseudorapidity range $|\eta| <$ 1.1 can be identified using the combined time-of-flight information from the TOF detector and the $dE/dx$ signal from TPC. Fig. 4 shows a typical

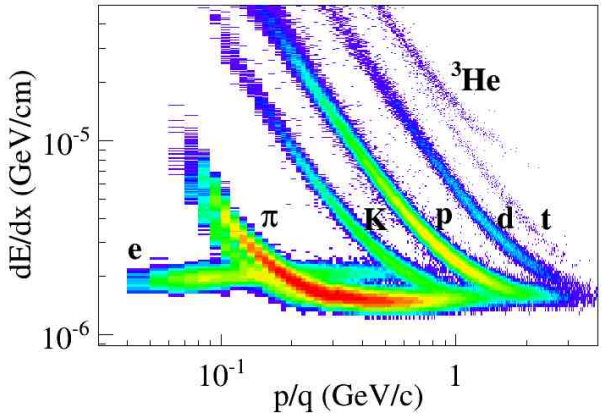


Fig. 3. Specific energy loss $dE/dx$ versus magnetic rigidity $p/q$ for $\pi$, $K$, $p$, $d$, $t$, $^3He$.

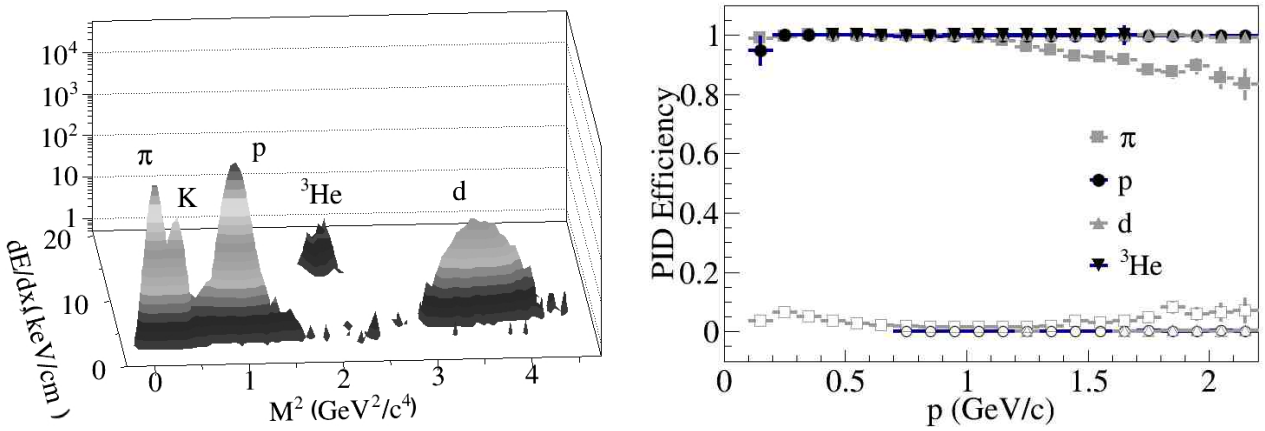


(a) (b)

Fig. 4. (a) Specific energy loss $dE/dx$ versus mass square $M^2$ for $\pi$, $K$, $p$, $d$, $t$,$^3He$ at $p = 1.5$ GeV/$c$. (b) PID efficiency (filled symbols) and contamination of mis-identified particles (empty symbols) as functions of the total momentum.

$dE/dx$ versus $M^2$ distribution for tracks with momentum $p = 1.5$ GeV/c.

Selected hadron and light nuclei candidates fall within the $3\sigma$ ellipses around the nominal position for a given particle type. In addition, the probability for a given particle to belong to each of the species can be calculated knowing the widths of the corresponding distributions (along the $dE/dx$ and $M^2$ axes) and the difference from the predicted position for the specie. It was found that by requiring this probability to be greater than 0.75 one can get the efficiency and contamination distributions shown on the (b) panel of Fig. 4. The PID efficiency is defined as a ratio of correctly tagged to the total number of generated particles. The contamination is determined as the number of incorrectly tagged particles divided by the number of correctly tagged particles.

As seen from Fig. 4, the overall PID efficiency for $p$, $d$ and $^3$He is close to 100%, while due to a partial overlap of the distributions for pions and kaons the efficiency of $\pi$ drops down to $\approx 0.8$ at $p = 2.5$ GeV/c. The contamination of wrongly identified pions (basically from $\mu$, $e$, and $K$) does not exceed 10%. For other species the observed contribution from the mis-identified particles is negligible.

## ANALYSIS PROCEDURE

$^3_\Lambda$H hypernuclei were reconstructed using their decay modes into two (2-prong $^3_\Lambda$H) or three (3-prong $^3_\Lambda$H) charged tracks. The signal event topology (decay of a relatively long-lived particle into two or more tracks - Fig. 5 ) defines the selection criteria: relatively large distance of the closest approach (DCA) to the primary vertex of decay products, small track-to-track separation in the decay vertex, relatively large decay length of the mother particle. Both the DCA and two-track separation cuts should be more efficient if applied in $\chi^2$ - space, i.e if normalized to their respective errors.

The exact values of selection cuts were found by performing a multidimensional scan over the whole set of selection criteria with a requirement to maximize the invariant mass peak significance, defined as $S/S+B$, where $S$ and $B$ are total numbers of signal (described the Gaussian) and background (polynomial function) combinations inside $2\sigma$ interval around the peak position.

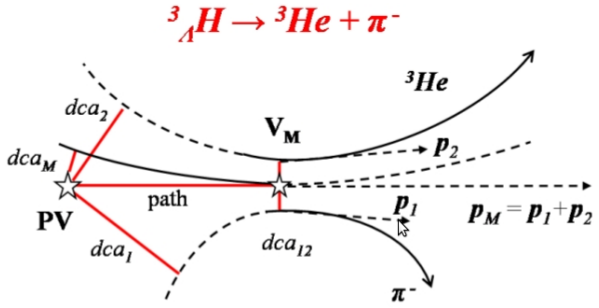


Fig. 5. Event topology of two-particle decays of a charged particle(e.g. $^3_\Lambda\mathrm{H} \rightarrow ^3 He + \pi^-$) (transverse view). Here $dca_1$ and $dca_2$ are the distances of the closest approach of the decay tracks to the primary vertex $PV$, $dca_{12}$ is the distance between daughter tracks in the decay vertex $V_M$, $dca_M$ is the distance of the closest approach of the mother particle to the primary vertex, path is the decay length, $p_1$ and $p_2$ are the momenta of daughter particles.

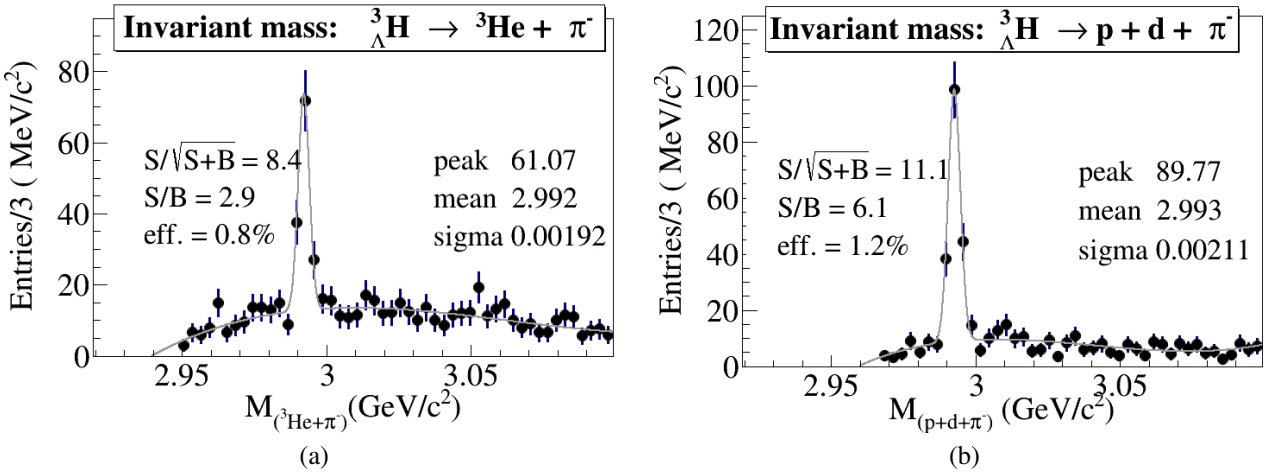


Fig. 6. (a) Reconstructed invariant mass of $^3He$ and $\pi^-$, (b) Reconstructed invariant mass of proton, deuteron and $\pi^-$ ($DCM-QGSM$ generator at $\sqrt{s}$ = 5A GeV).

The corresponding scan procedure was realized as follows: during the particle combinations the parameters which have been chosen to serve as selection criteria (see above) were recorded along with the invariant mass value. Later, multiple loops over those variables were performed in some steps and their values were used as low or high thresholds, yielding the invariant mass peak significance for each set of selection cut values. Then, the maximum value was taken along with the corresponding set of selection parameters.

## RESULTS

The results on $^3_\Lambda$H reconstruction are presented in Fig. 6 and Tab. 2. Figure 6 shows invariant mass distributions for 2-prong ($^3_\Lambda\mathrm{H} \rightarrow ^3 He + \pi^-$) and 3-prong ($^3_\Lambda\mathrm{H} \rightarrow p + d + \pi^-$) decay modes. As mentioned above, the results have been obtained for $5 \cdot 10^5$ central events, corresponding to about 30 minutes of NICA running time. One can see narrow peaks ($\sigma$ of the Gaussian fit $\approx$2 MeV/$c^2$) with quite high significance and signal-to-background ratio.

Table 2 shows the effect of the detector acceptance (i.e. $\eta$-coverage and low-$p_T$ cut for $^3_\Lambda$H decay products) on hypertriton detection efficiency, where the efficiency is defined with respect to the total number of hypernuclei. Lines 2-5 demonstrate the effect of the $p_T$-cut on the efficiency, where $p_T$ is the true transverse momentum of decay products. Line 6 shows the reconstruction efficiency, i.e. considering the reconstructed in the detector decay particles without any explicit $p_T$-cut (and without PID efficiency). The last line includes all the relevant factors, i.e. reconstruction and PID efficiencies as well as selection efficiency. One can see that the detector provides rather efficient reconstruction of hypertritons with $p_T$ of decay tracks above 0.1 GeV/$c$ in good agreement with Fig. 1. It is also clear that a higher $p_T$-threshold (e.g. 0.2 GeV/$c$) would significantly reduce the detector efficiency. The efficiency drop due to selection cuts

Table 2. Factors affecting $^3_\Lambda$H reconstruction efficiency

| Factor | Efficiency, % | |
|---|---|---|
| | 2-prong decay | 3-prong decay |
| Branching ratio | 24.6 | 36.4 |
| Decay products at $\|\eta\| < 1.3$ | 14.9 | 19.8 |
| Decay products at $\|\eta\| < 1.3$ and $p_T > 0.05$ GeV/$c$ | 14.2 | 15.7 |
| Decay products at $\|\eta\| < 1.3$ and $p_T > 0.1$ GeV/$c$ | 8.9 | 6.2 |
| Decay products at $\|\eta\| < 1.3$ and $p_T > 0.2$ GeV/$c$ | 0.7 | 0.1 |
| Reconstructed decay products at $\|\eta\| < 1.3$ | 7.9 | 8.3 |
| Maximum siginificance | 0.8 | 1.2 |

comes from the necessity to suppress the combinatorial background in order to obtain a clean invariant mass peak.

## SUMMARY

We have performed a simulation study of the MPD detector capabilities to reconstruct hypertritons ${}^{3}_{\Lambda}$H in central Au+Au collisions at $\sqrt{s}$ =5A GeV. The DCM-QGSM event generator was used as the input for the study of the MPD detector set-up comprising the Time Projection Chamber and barrel Time-Of-Flight system. Particle identification was achieved by combining the energy loss (from TPC) and time-of-flight (from TOF) measurements. A special procedure aimed at the maximization of the significance of the reconstructed invariant mass was developed resulting in the observed signal-to-background ratio $S/B = 3-6$ for hypertritons. The invariant mass resolution of $\approx$2 MeV/$c^2$ has been achieved. Based on the results of this study and model predictions, we have estimated the expected yield of ${}^{3}_{\Lambda}$H for 10 weeks of data taking as $9 \cdot 10^5$ particles.

It is planned to develop a reconstruction algorithm for double-strange nuclei ${}^{4}_{\Lambda\Lambda}$H and ${}^{5}_{\Lambda\Lambda}$H.

## REFERENCES


[1] A.N. Sissakian and A.S. Sorin, *J. Phys. G: Nucl. Part. Phys.* **36**, 064069 (2009).

[2] R. Rapp, G. Chanfray and J. Wambach, *Phys. Rev. Lett.* **76**, 368 (1996).

[3] R. Rapp and J. Wambach, *Adv. Nucl. Phys.* **25**, 1 (2000).

[4] T. Hatsuda and S. H. Lee, *Phys. Rev. C* **46**, 34 (1992).

[5] C. Alt et al., *Phys. Rev. C* **78**, 024903 (2008).

[6] L. Kumar (STAR Collaboration), *J. Phys. G: Nucl. Part. Phys.* **38**, 124145 (2011).

[7] J. Randrup and J. Cleymans, *Phys. Rev. C* **74**, 047901 (2006).

[8] http://nica.jinr.ru/files/NICA CDR.pdf, last access: 31.10.2014.

[9] K.U. Abraamyan et al., *Nucl. Instrum. Meth. A* **628**, 99 (2011).

[10] http://nica.jinr.ru/files/CDR MPD/MPD CDR en.pdf, last access: 31.10.2014.

[11] A.K. Kermann and M.S. Weiss, *Phys. Rev. C* **8**, 408 (1973).

[12] The STAR Collaboration, *Science* **328**, 58 (2010).

[13] B. Dönigus (ALICE Collaboration), *Nucl. Phys. A* **904-905**, 547 (2013).

[14] M. Wakai, H. Bando and M. Sano, *Phys. Rev. C* **38**, 748 (1998).

[15] A. Andronic et al., *Phys. Lett. B* **697**, 203 (2011).

[16] J. Steinheimer et al., *Phys. Lett. B* **714**, 85 (2012).

[17] V.D. Toneev and K.K. Gudima, *Nucl. Phys. A* **400**, 173 (1983).

[18] V.D. Toneev et al., *Nucl. Phys. A* **519**, 463 (1990).

[19] N.S. Amelin et al., *Sov. J. Nucl. Phys.* **52**, 272 (1990).

[20] T.A. Armstrong et al. (E864 Collaboration), *Phys. Rev. Lett.* **83**, 5431 (1999).

[21] T.A. Armstrong et al. (E864 Collaboration), *Phys. Rev. C* **61**, 064908 (2000).

[22] H. Kamada et al., *Phys. Rev. C* **57**, 1595 (1998).

[23] R. Fruehwirth, *Nucl. Instr. and Meth. A* **262**, 444 (1987).

[24] R. Luchsinger and Ch. Grab, *Comp. Phys. Comm.* **76**, 263 (1993).

[25] J. Beringer et al. (Particle Data Group), *Phys. Rev. D* **86**, 010001 (2012).

# ИЗУЧАВАНЕ И РЕКОНСТРУКЦИЯ НА ХИПЕРЯДРА КЪМ ПРОЕКТА NICA/MPD

М. Илиева, В. Колесников, Д. Сувариева, В. Васендина, Ал. Зинченко

*Обединен институт за ядрени изследвания,*
*ул. "Жолио Кюри" №6, Дубна, Московская область, 141980, Русия*

(Резюме)

Хиперядрата се получават при хиперон-нуклонни взаимодействия. Това са ядра съдържащи поне един допълнителен хиперон към нуклоните. Ние изучавахме разпада на най-лекото хиперядро: хипертритон на $^{3}$He+$\pi^{-}$.

Изследване получаването на леки хиперядра е от съществено значение за разбирането на механизма на производството на екзотични обекти, като мултихиперядра. Също така ще ни помогне да разберем странните степени на свобода в адронни системи.

Възможността да произвеждаме хиперядра ще ни позволи да изследваме всички населени региони в триизмерната ядрена карта.